$Na_3V(PO_4)_2$ cathode material for Na ion batteries: Defects, dopants and Na diffusion

Navaratnarajah Kuganathan[1,2,a)] and Alexander Chroneos[1,2,b)]

[1]Department of Materials, Imperial College London, London, SW7 2AZ, United Kingdom

[2]Faculty of Engineering, Environment and Computing, Coventry University, Priory Street, Coventry CV1 5FB, United Kingdom

---

Abstract

Layered $Na_3V(PO4)_2$ has been recently identified as a high rate cathode material for Na ion batteries. We use atomistic simulation based on the classical pair potentials to calculate the most favourable intrinsic defect process, Na migration paths and tetravalent dopant incorporation at V and P sites. The Na-V anti-site defect is the most energetically favourable defect process. The Na Frenkel is the second most favourable intrinsic defect but only higher by 0.19 eV than the anti-site. Two dimensional long range Na ion migration with activation energy of 0.59 eV is observed along the *ab* plane implying that $Na_3V(PO_4)_2$ could be a promising cathode material for Na ion batteries. The formation of both Na vacancy and interstitial defects can be simultaneously achieved by substituting Ge on the V site and the P site required for vacancy migration and storage capacity respectively. High exoergic solution energy is calculated for La on the V site suggesting that the formation of $Na_3(V_xLa_{1-x})(PO_4)_2$ composition should be experimentally possible.

Keywords: $Na_3V(PO_4)_2$; Defects; Na diffusion; Dopants

[1]Corresponding authors, e-mails: a) n.kuganathan@imperial.ac.uk ; b) alexander.chroneos@imperial.ac.uk

1. Introduction

Growing energy demand arising from non-renewable fossil fuels requires high capacity energy storage systems. Lithium ion batteries (LIBs) are promising candidate devices that have been successfully developed and commercialized for small-scale applications. Low abundance of lithium and its unequal distribution in the earth's crust led to a significant challenge in constructing LIBs needed for large-scale applications such as hybrid electric vehicles. Sodium ion batteries (SIBs) are being actively considered as an alternative to LIBs owing to unlimited resource of Na found worldwide, low cost and similar energy storage mechanism to LIBs [1-3]. High natural abundance of Na is an advantage of designing electrode materials for large-scale NIBs.

Sodium based materials [4-8] including $NaMO_2$ (M=Fe, Mn, Co, V, Cr, Ti and Ni)[9-15], $NaFePO_4$ [9], $Na_3Ni_2BiO_6$ [16] and Na_2CoSiO_4 [17] have been considered as promising electrode materials for SIBs. The development of novel materials is required to provide better electrochemical performance and capacity than that of existing materials with the aim of applying those materials in high energy storage systems such as electrical vehicles.

A novel layered type $Na_3V(PO_4)_2$ has been recently introduced as a high voltage cathode material for NIBs [18,19]. As this material consists of polyanionic orthophosphate (PO_4^{3-}) groups with strong P–O bonds, good structural stability and reasonably high redox potentials are expected. Furthermore, variable oxidation states of vanadium (from +2 to +5) is an advantage of exhibiting good redox reactions by forming different V-based polyhedral structures. Kim *et al.*[18] reported the synthesis of $Na_3V(PO_4)_2$ using X-ray diffraction first time. Their study exhibited outstanding power capability (~79% of the theoretical capacity at 15 C) and excellent cyclability. Very recently Kovrugin *et al.*[19] synthesised $Na_3V(PO_4)_2$ and showed that as-prepared material can provide high voltage plateaus around 3.6 and 4.0 V vs Na^+/Na. Furthermore, a high theoretical capacity of 173 mAh/g with a possible two electron transfer per V is expected. There are only a very few theoretical studies available on this new cathode material in the literature. Density functional theory calculations performed by Kim *et al.*[18] show that two dimensionally connected Na diffusion path with activation energy of 0.433 eV is present. The bond valence energy landscape method was used by Kovrugin *et al.*[19] to calculate the activation energies of Na ion diffusion in $Na_3V(PO_4)_2$. High activation energies (from 1.6 eV to 5.5 eV) were reported for local Na hops meaning that Na ion migration in this material is expected to be slow.

In the present study, we have used well-established atomistic simulations based on the interatomic potentials to examine the defect processes, Na self-diffusion and dopant properties in $Na_3V(PO_4)_2$ in order to optimize this material in rechargeable Na ion batteries. The current computational modelling technique has been successfully applied to various battery materials [20-33] and can be useful to future experimental work providing defect energetics, diffusion mechanisms and promising dopants to be considered in $Na_3V(PO_4)_2$.

2. Computational Methods

All calculations were performed using the GULP code [34] which is associated with the classical Born model description of ionic solids. In this method, long-range Coulombic interactions and short-range repulsive interactions representing electron-electron repulsion and van der Waals interactions were used to model interactions between ions. Short range interactions were modelled using Buckingham potentials (Table S1). Geometry optimisation (both atom positions and lattice constants) was performed using the Broyden-Fletcher-Goldfarb-Shanno (BFGS) algorithm [35]. A supercell containing 603 atoms was used for all defect calculations. In all calculations, a gradient norm of 0.001 eV/Å was used to convergence both non-defect and defect structures. Mott-Littleton method [36] was used to model lattice relaxations around point defects and the migrating ions. The local maximum energy along the diffusion path was considered as the activation energy of migration. As the present model assumes a full charge ionic model within the dilute limit, the defect energies will be overestimated but the trend will be consistent. Thermodynamically the migration and formation energies (i.e. the defect parameters) may be defined with the comparison of the real defective crystal to an isochoric or isobaric (as in the present study as well as elsewhere, e.g., see ref 37) non-defective crystal and be interconnected via thermodynamic relations [38-41].

3. Results and discussion

3.1. $Na_3V(PO_4)_2$ crystal structure

Figure 1 exhibits the crystal structure of monoclinic $Na_3V(PO_4)_2$ (space group $C/2c$, lattice parameters a=9.104 Å, b=5.037 Å, c=13.851 Å, α=90°, β=91.258° and γ=90°) as reported by Kovrugin *et al.*[19] in their experiment. Vanadium and phosphorous form VO_6 octahedron and PO_4 tetrahedron with adjacent oxygen atoms respectively (refer to Figure 1). The VO_6 octahedra and PO_4 tetrahedra share their corners to form a VO_6-PO_4 layer along the *ab* plane. Sodium atoms occupy sites in two different interlayers along the *ab* plane enabling Na ions to migrate *via* two dimensional channels. Here we employed classical

potentials based atomistic simulation to reproduce the experimental crystal structure of $Na_3V(PO_4)_2$ with well-established pair potentials available in the literature (see Table S1 in the supplementary potential information). There is an excellent agreement between the calculated and experimental structural parameters within a margin of ~1% error (see Table 1).

3.2. Intrinsic defects

We calculated Frenkel, Schottky and anti-site defect energies. These defect energies were calculated by combining isolated point defects (vacancy and interstitial) and are useful to understand the electrochemical behaviour of $Na_3V(PO_4)_2$. The intrinsic defect reactions (Eqs.1-8) for Frenkel, Schottky and anti-site defects are given below using Kröger-Vink notation [42].

$$\text{Na Frenkel: } Na_{Na}^{X} \rightarrow V'_{Na} + Na_i^{\bullet\bullet} \quad (1)$$

$$\text{O Frenkel: } O_O^{X} \rightarrow V_O^{\bullet\bullet} + O_i'' \quad (2)$$

$$\text{V Frenkel: } V_V^{X} \rightarrow V_V''' + V_i^{\bullet\bullet\bullet} \quad (3)$$

$$\text{Schottky: } 3Na_{Na}^{X} + V_V^{X} + 2P_P^{X} + 8O_O^{X} \rightarrow 3V'_{Na} + V_V''' + 2V_P'''' + 8V_O^{\bullet\bullet} + Na_3V(PO_4)_2 \quad (4)$$

$$\text{Na}_2\text{O Schottky: } 2\,Na_{Na}^{X} + O_O^{X} \rightarrow 2\,V'_{Na} + V_O^{\bullet\bullet} + Na_2O \quad (5)$$

$$\text{V}_2\text{O}_3 \text{ Schottky: } 2\,V_V^{X} + 3\,O_O^{X} \rightarrow 2\,V_V'''' + 3\,V_O^{\bullet\bullet} + V_2O_3 \quad (6)$$

$$\text{Na/V antisite (isolated): } Na_{Na}^{X} + V_V^{X} \rightarrow Na_V'' + V_{Na}^{\bullet\bullet} \quad (7)$$

$$\text{Na/V antisite (cluster): } Na_{Na}^{X} + V_V^{X} \rightarrow \{Na_V'': V_{Na}^{\bullet\bullet}\}^{X} \quad (8)$$

Intrinsic defect reaction energies were calculated (refer to Figure 2). The Na-V anti-site defect cluster (equation 8) is the lowest energy defect process (1.22 eV/defect) meaning that a small percentage of cation mixing will be present at high temperatures though the exact concentration is not known. This defect has been found both experimentally and theoretically in both Li and Na ion battery materials [20-33, 43-46]. The isolated form of anti-site defect (2.24 eV/defect) means that both isolated defects (Na_V'' and $V_{Na}^{\bullet\bullet}$) were calculated separately and their energies were combined. The cluster form of anti-site defect (equation 8) was calculated considering both isolated defects close to each other in the lattice. The binding energy for the formation of this anti-site cluster from isolated anti-site defects is calculated to be −1.02 eV/defect. The exoergic binding is due to the strong attraction between oppositively charged isolated defects. The Na Frenkel (1.42 eV/defect) is the second most favourable defect process. The Na Frenkel is higher only by 0.19 eV/defect

than the anti-site defect. The Na_2O Schottky-like reaction (relation 5) leading to the formation of further V'_{Na} and $V_O^{\bullet\bullet}$ is calculated to be 2.27 eV per defect, implying that this process may also take place at elevated temperatures. The reaction energies for the P Frenkel, the V Frenkel, the O Frenkel and Schottky defects are even higher suggesting that they are unlikely to occur.

3.3. Na ion diffusion

Na ion diffusion with low activation energy is a key requirement for a promising cathode material. The current methodology allowed the identification of various possible Na ion diffusion paths together with activation energies in $Na_3V(PO_4)_2$. Using experimental techniques it is often difficult to observe Na ion diffusion pathways and calculate activation energies. The current modelling technique has been successfully used to determine various ionic transport paths in different ionic materials including Na and Li ion battery materials. For example, the lithium ion migration path calculated in $LiFePO_4$ using classical pair potentials [47] was exactly observed later in the high-temperature powder neutron diffraction and the maximum entropy method [48]. A curved one-dimensional chain for lithium motion with Li-Li separation of 3.01 Å was clearly visualized along [010] direction in the experiment. In our previous study [25], we have shown that three dimensional long range Na ion pathway can be observed in Na_2MnSiO_4.

Three different Na diffusion local Na hops (refer to Figure 3) were identified. Table 2 reports the activation energies together with the Na-Na separation. Energy profile diagrams for each Na hops are shown in Figure 4. Possible long-range paths were also constructed by connecting local Na hops. We identified three long-range three dimensional paths (see Figure 3). In the first long range path (along the *ab* plane), Na ion migrates *via* a zig-zag pattern (B→C→C→B) with the lowest overall activation energy of 0.59 eV. In the second and the third long-range paths [(A→B→A→B) and (A→C→A→C), Na ion moves via *ab* plane, but the overall activation energies are the same (0.71 eV) due to the involvement of local hop A, which has an activation energy of 0.71 eV. The low activation energy of 0.59 eV indicates that high lithium ionic conductivity in this material would be observed. The current activation energy (0.59 eV) value is in agreement with the value (0.433 eV) obtained by Kim *et al.* [18] in their DFT simulations. Such difference is due to the two different methodologies. Nevertheless, Na ion diffusion in this material would be high.

4. Dopant substitution

We considered isovalent dopants on the V site and tetravalent dopants on both V and P sites. Tetravalent dopants substitution required charge-compensation in the form of vacancies and interstitials. Appropriate lattice energies (calculated using the same potentials) were also calculated and used.

First, tetravalent dopants (Si, Ge, Ti, Sn and Ce) were considered on the V site. The following reaction was used to calculate solution energies:

$$2\,MO_2 + 2\,V_V^X + 2\,Na_{Na}^X \rightarrow 2M_V^{\bullet} + 2\,V'_{Na} + V_2O_3 + Na_2O \qquad (9)$$

The lowest solution energy is calculated for Ge (see Figure 5). The solution energy calculated for Sn is only higher by 0.05 eV compared that of Ge. Both Ti and Ce exhibit high solution energies, whereas the incorporation of Si^{4+} is highly unfavourable.

Next, we considered the incorporation of M^{4+} ions on the P site with Na interstitials as charge-compensating defects (equation 10).

$$2\,MO_2 + 2\,P_P^X + Na_2O \rightarrow 2M'_P + 2\,Na_i^{\bullet} + P_2O_5 \qquad (10)$$

Doping of M^{4+} ions on the P site introduces Na interstitials enhancing the capacity in $Na_3V(PO_4)_2$ required for large scale applications. The most favourable dopant for this process is Si^{4+} (see Figure 5). The solution energy gradually increases with ionic radius. Doping of Ce^{4+} is unlikely to occur due to the high solution energy (9.62 eV/defect). Finally, isovalent dopants (Al, Ga, Sc, In, Y, Gd and La) were considered on the V site. The following reaction was used to calculate the solution energy:

$$M_2O_3 + 2\,V_V^X \rightarrow 2M_V^x + V_2O_3 \qquad (11)$$

Exoergic solution energies are observed for most of the dopants except for Al and Ga (refer to Figure 6). Interestingly, La exhibits high negative solution energy indicating that the experimental investigation of this dopant should be carried out.

Conclusions

The present study aimed to understand the defect chemistry, Na ion migration and the dopant properties in $Na_3V(PO_4)_2$ using well-established atomistic simulation technique. The Na-V anti-site defect is found to be the most dominant defect. Two dimensional Na ion migration along the *ab* plane with the activation energy of 0.59 eV indicates that this material would exhibit high ionic conductivity. The tetravalent dopant Ge^{4+} on the V site would increase the concentration of Na vacancy needed for Na ion migration while the same dopant on the P site would increase the Na content in the form of Na interstitial needed for

capacity. Isovalent dopant La seems to be promising candidate for the formation of $Na_3(V_xLa_{1-x})(PO_4)_2$.

Acknowledgements

Computational facilities and support were provided by High Performance Computing Centre at Imperial College London. The research leading to these results has received funding from the European Union's H2020 Programme under Grant Agreement no 824072– HARVESTORE.

Competing interests: The authors declare no competing interests.

References

1. B.L. Ellis, L.F. Nazar, Current Opinion in Solid State and Materials Science 16 (2012) 168.

2. N. Yabuuchi, K. Kubota, M. Dahbi, S. Komaba, Chemical Reviews 114 (2014) 11636.

3. V. Palomares, M. Casas-Cabanas, E. Castillo-Martínez, M.H. Han, T. Rojo, Energy & Environmental Science 6 (2013) 2312.

4. S.-M. Oh, S.-T. Myung, J. Hassoun, B. Scrosati, Y.-K. Sun, Electrochemistry Communications 22 (2012) 149.

5. Y. Fang, Q. Liu, L. Xiao, X. Ai, H. Yang, Y. Cao, ACS Applied Materials & Interfaces 7 (2015) 17977.

6. W. Tang, X. Song, Y. Du, C. Peng, M. Lin, S. Xi, B. Tian, J. Zheng, Y. Wu, F. Pan, K.P. Loh, Journal of Materials Chemistry A 4 (2016) 4882.

7. Y. Kawabe, N. Yabuuchi, M. Kajiyama, N. Fukuhara, T. Inamasu, R. Okuyama, I. Nakai, S.
Komaba, Electrochemistry Communications 13 (2011) 1225.

8. N.V. Kosova, V.R. Podugolnikov, E.T. Devyatkina, A.B. Slobodyuk, Materials Research Bulletin 60 (2014) 849.

9. P. Vassilaras, X. Ma, X. Li, G. Ceder, Journal of The Electrochemical Society 160 (2013) A207.

10. X. Ma, H. Chen, G. Ceder, Journal of The Electrochemical Society 158 (2011) A1307.

11. S. Komaba, C. Takei, T. Nakayama, A. Ogata, N. Yabuuchi, Electrochemistry Communications 12 (2010) 355.

12. C. Didier, M. Guignard, C. Denage, O. Szajwaj, S. Ito, I. Saadoune, J. Darriet, C. Delmas, Electrochemical and Solid-State Letters 14 (2011) A75.

13. D. Wu, X. Li, B. Xu, N. Twu, L. Liu, G. Ceder, Energy & Environmental Science 8 (2015)

195.

14. A. Maazaz, C. Delmas, P. Hagenmuller, Journal of inclusion phenomena 1 (1983) 45.

15. Y. Takeda, K. Nakahara, M. Nishijima, N. Imanishi, O. Yamamoto, M. Takano, R. Kanno,

Materials Research Bulletin 29 (1994) 659.

16. D.S. Bhange, G. Ali, D.-H. Kim, D.A. Anang, T.J. Shin, M.-G. Kim, Y.-M. Kang, K.Y.

Chung, K.-W. Nam, Journal of Materials Chemistry A 5 (2017) 1300.

17. J.C. Treacher, S.M. Wood, M.S. Islam, E. Kendrick, Physical Chemistry Chemical Physics

18 (2016) 32744.

18. J. Kim, G. Yoon, H. Kim, Y.-U. Park, K. Kang, Chemistry of Materials 30 (2018) 3683.

19. V.M. Kovrugin, R. David, J.-N. Chotard, N. Recham, C. Masquelier, Inorganic Chemistry

57 (2018) 8760.

20. N. Kuganathan, M.S. Islam, Chemistry of Materials 21 (2009) 5196.

21. A.R. Armstrong, N. Kuganathan, M.S. Islam, P.G. Bruce, Journal of the American

Chemical Society 133 (2011) 13031.

22. C.A.J. Fisher, N. Kuganathan, M.S. Islam, Journal of Materials Chemistry A 1 (2013) 4207.

23. N. Kuganathan, A. Kordatos, S. Anurakavan, P. Iyngaran, A. Chroneos, Materials

Chemistry and Physics 225 (2019) 34.

24. A. Kordatos, N. Kuganathan, N. Kelaidis, P. Iyngaran, A. Chroneos, Scientific Reports 8

(2018) 6754.

25. N. Kuganathan, A. Chroneos, Scientific Reports 8 (2018) 14669.

26. N. Kuganathan, S. Ganeshalingam, A. Chroneos, Scientific Reports 8 (2018) 8140.

27. N. Kuganathan, P. Iyngaran, A. Chroneos, Scientific Reports 8 (2018) 5832.

28. N. Kuganathan, A. Kordatos, A. Chroneos, Scientific Reports 8 (2018) 12621.

29. N. Kuganathan, A. Kordatos, M.E. Fitzpatrick, R.V. Vovk, A. Chroneos, Solid State Ionics

327 (2018) 93.

30. N. Kuganathan, A. Kordatos, A. Chroneos, Scientific Reports 9 (2019) 550.

31. N. Kuganathan, A. Chroneos, Scientific Reports 9 (2019) 333.

32. N. Kuganathan, A. Kordatos, N. Kelaidis, A. Chroneos, Scientific Reports 9 (2019) 2192.

33. N. Kuganathan, L.H. Tsoukalas, A. Chroneos, Solid State Ionics 335 (2019) 61.

34. J.D. Gale, A.L. Rohl, Molecular Simulation 29 (2003) 291.

35. J.D. Gale, Journal of the Chemical Society, Faraday Transactions 93 (1997) 629.

36. N.F. Mott, M.J. Littleton, Transactions of the Faraday Society 34 (1938) 485.

37. P. Varotsos, Solid State Ionics 179 (2008) 438.
38. P. Varotsos, Phys. Rev. B 76 (2007) 092106 .
39. P. Varotsos, J. Appl. Phys. 101 (2007) 123503.
40. A. Chroneos and R.V. Vovk, Solid State Ionics 274 (2015) 1-3
41. A. Chroneos, Appl. Phys. Rev. 3 (2016) 041304.
42. F.A. Kröger, H.J. Vink, in: F. Seitz, D. Turnbull (Eds.), Solid State Physics, Academic Press, 1956, p. 307.
43. V.V. Politaev, A.A. Petrenko, V.B. Nalbandyan, B.S. Medvedev, E.S. Shvetsova, Journal of Solid State Chemistry 180 (2007) 1045.
44. A. Nytén, A. Abouimrane, M. Armand, T. Gustafsson, J.O. Thomas, Electrochemistry Communications 7 (2005) 156.
45. D. Ensling, M. Stjerndahl, A. Nytén, T. Gustafsson, J.O. Thomas, Journal of Materials Chemistry 19 (2009) 82.
46. M. Kempaiah Devaraju, Q. Duc Truong, H. Hyodo, Y. Sasaki, I. Honma, Scientific Reports 5 (2015) 11041.
47. M.S. Islam, D.J. Driscoll, C.A.J. Fisher, P.R. Slater, Chemistry of Materials 17 (2005) 5085.
48. S.-i. Nishimura, G. Kobayashi, K. Ohoyama, R. Kanno, M. Yashima, A. Yamada, Nature Materials 7 (2008) 707.

Table 1. Calculated structural parameters and corresponding experimental values reported for monoclinic $(C/2c)$ $Na_3V(PO_4)_2$.

Parameter	Calc	Expt[19]	$\|\Delta\|$(%)
a (Å)	9.011	9.104	1.03
b (Å)	5.089	5.037	1.03
c (Å)	13.940	13.851	0.64
α (°)	90.00	90.00	0.00
β (°)	90.464	91.258	0.87
γ (°)	90.00	90.00	0.00
V (Å^3)	639.22	635.04	0.66

Table 2. Calculated Na-Na separations and activation energies using classical pair-potential method for the Na-ion migration between two adjacent Na sites (refer to Figure 3).

Migration path	Na-Na separation (Å)	Activation energy (eV)
A	3.30	0.71
B	3.40	0.56
C	3.43	0.59

Table 3. Possible long-range Na ion diffusion paths and their corresponding overall activation energies.

Long-range path	Overall activation energy (eV)
B→C→C→ B	0.59
A→B→A→B	0.71
A→C→A→C	0.71

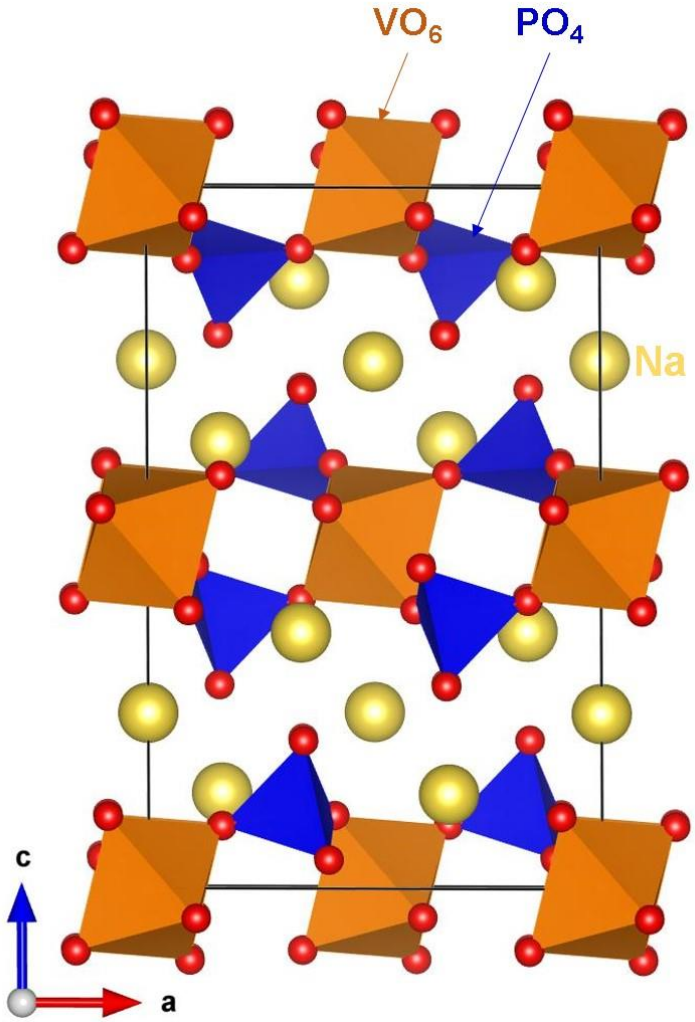

Figure 1. Crystal structure of monoclinic $Na_3V(PO_4)_2$ (space group $C2/c$)

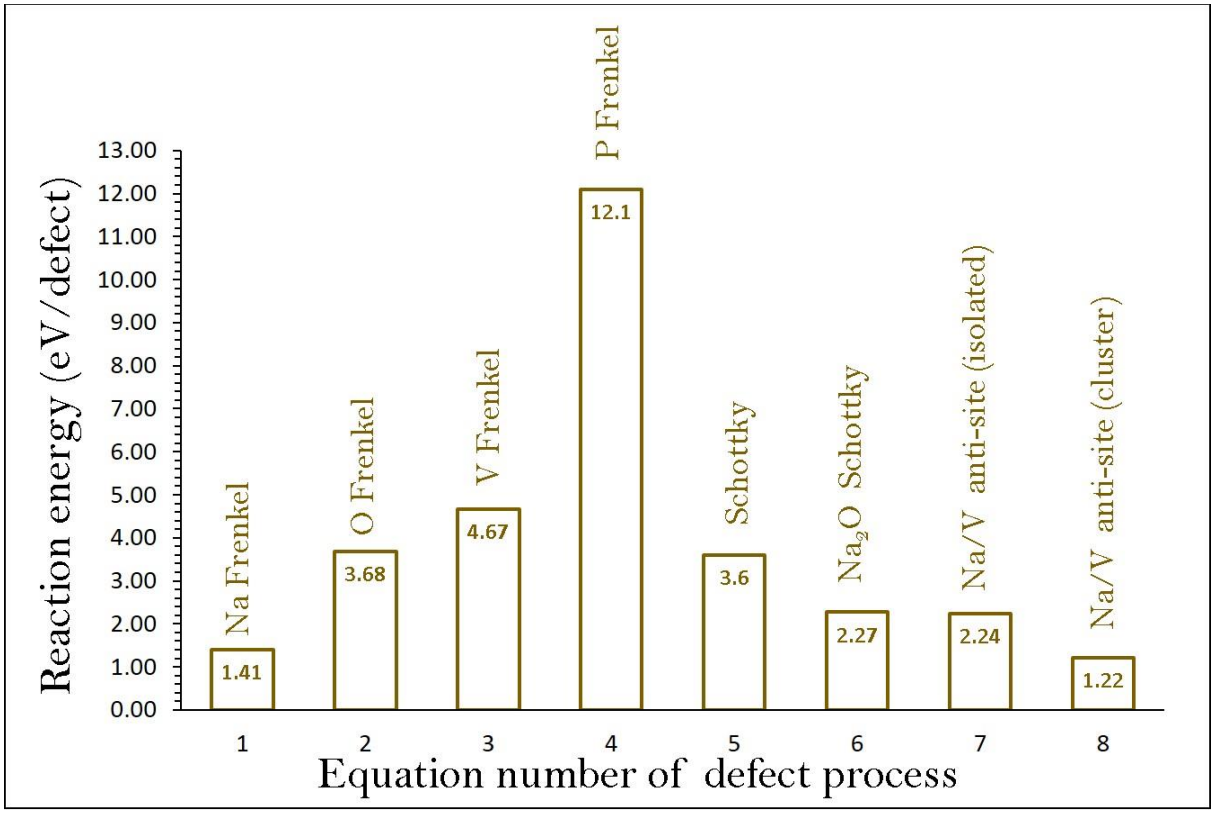

Figure 2. Energetics of intrinsic defect process calculated in monoclinic $Na_3V(PO_4)_2$.

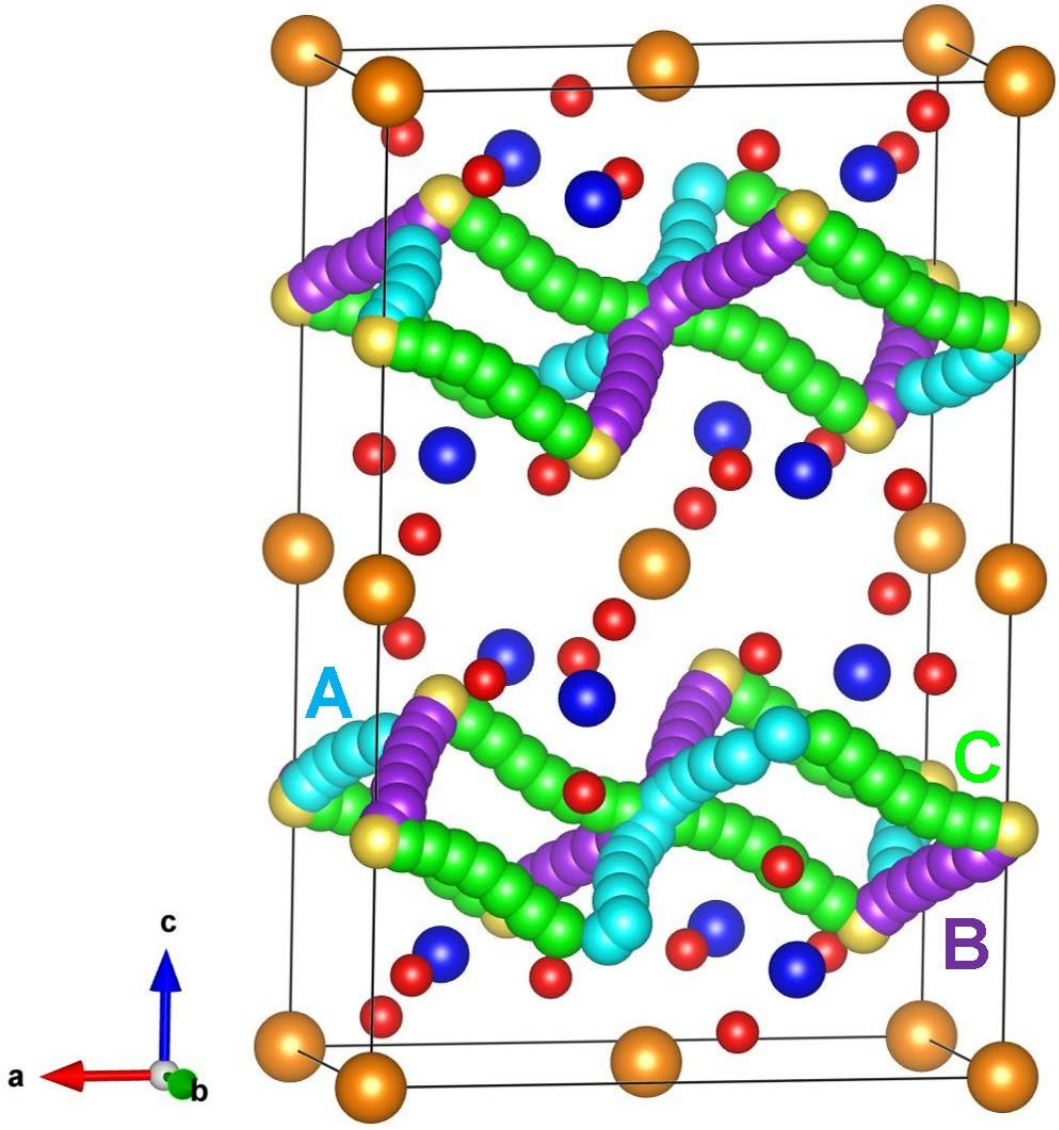

Figure 3. Possible long-range sodium vacancy migration paths considered. Green, blue and purple colour atoms correspond to different Na hopping trajectories.

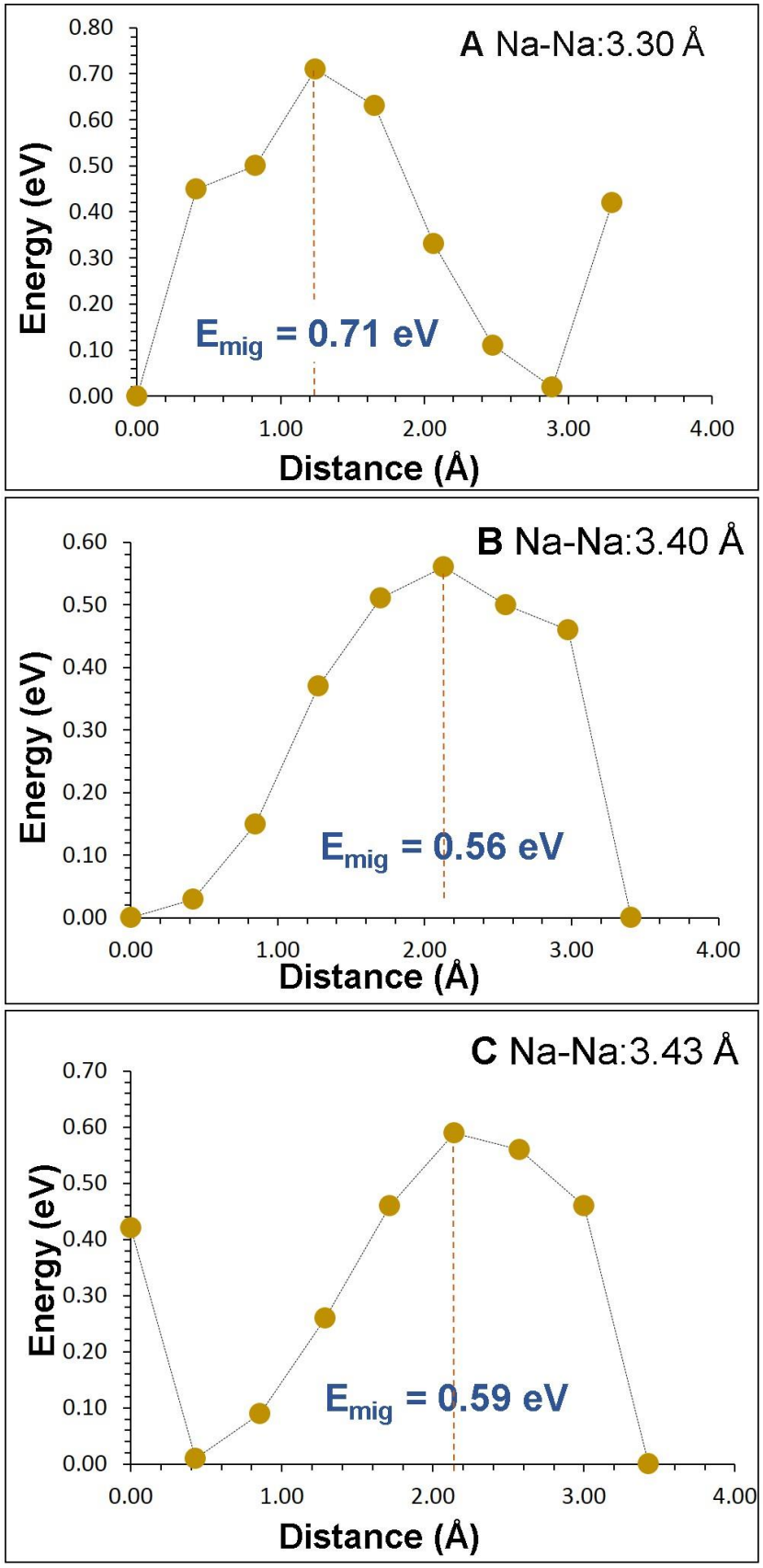

Figure 4. Three different energy profiles [as shown in Figure 3] of Na vacancy hopping between two adjacent Na sites in $Na_3V(PO_4)_2$.

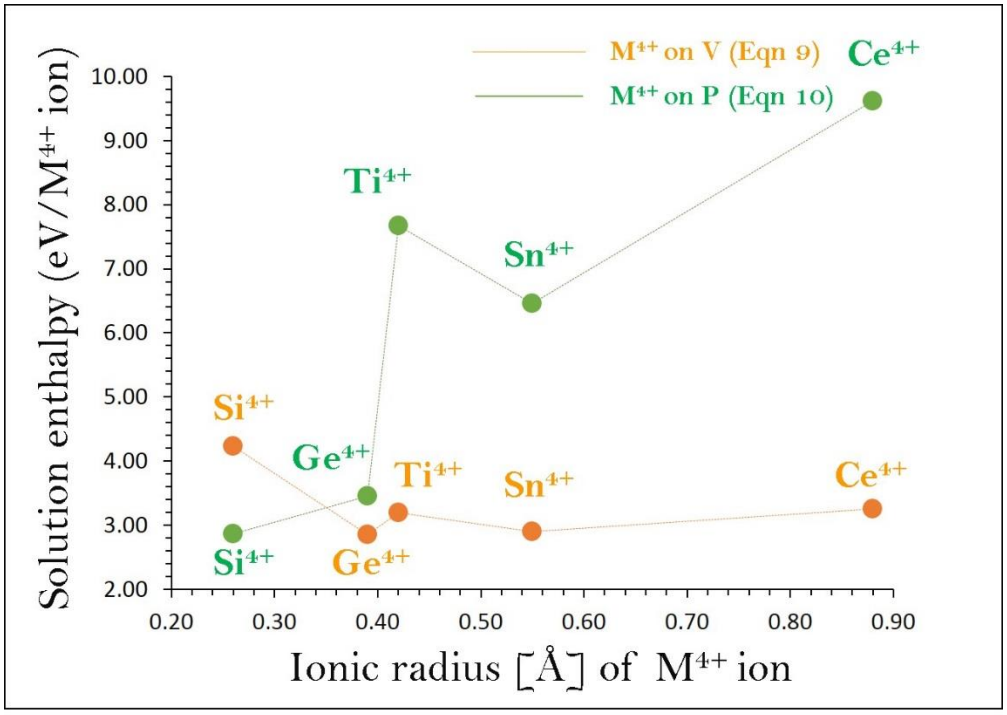

Figure 5. Enthalpy of solution of MO_2 (M = Si, Ge, Ti, Sn and Ce) with respect to the M^{4+} ionic radius in $Na_3V(PO_4)_2$.

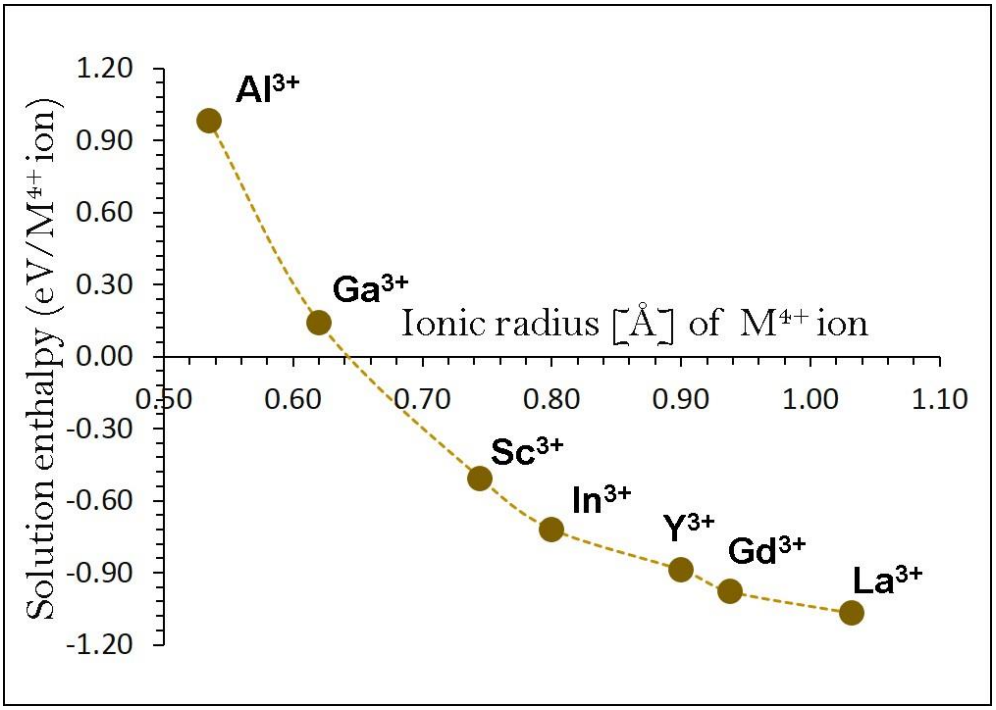

Figure 6. Enthalpy of solution of M_2O_3 (M = Al, Ga, Sc, In, Y, Gd and La) with respect to the M^{3+} ionic radius in $Na_3V(PO_4)_2$.